The spatial relationships between dissipation and production rates and vortical structures in turbulent boundary and mixing layers

James Diorio
Department of Mechanical Engineering, University of Maryland, College Park, Maryland 20742

Douglas H. Kelley
Institute for Research in Electronics and Applied Physics, University of Maryland, College Park, Maryland 20742

James M. Wallace[a)]
Department of Mechanical Engineering, University of Maryland, College Park, Maryland 20742

(Received 9 August 2006; accepted 21 December 2006; published online 5 March 2007)

A novel approach for studying the spatial relationship between the production and dissipation rates of turbulent kinetic energy and vortical structures is presented. Two turbulent flows were investigated: the zero pressure gradient boundary layer and the two-stream mixing layer. In both flows, a multisensor hot-wire probe was used to measure the velocity components in all three coordinate directions, as well as six components of the velocity gradient tensor. The remaining three velocity gradients were determined using Taylor's hypothesis. With these data, the "instantaneous" production and dissipation rates, defined by $P=-(\partial\bar{U}_i/\partial x_j)u_iu_j$ and $D=-\nu[(\partial u_i/\partial x_j)^2+(\partial u_i/\partial x_j)\times(\partial u_j/\partial x_i)]$, respectively, were determined. Cross-correlating the fluctuations of these two signals reveals that they are not randomly distributed in time with respect to each other; rather they display significant levels of correlation. Plotting the cross-correlation coefficients versus a dimensionless length scale, defined as $L'=\mathrm{sgn}(\tau)\sqrt{|\tau|/\nu\bar{U}}$, reveals an asymmetric pattern that persists at several cross-stream locations for both flows. Furthermore, correlating both the dissipation and production rates with a vortex identifier, $\omega_{xy}=[(\omega_x)^2+(\omega_y)^2]^{1/2}$, also reveals consistent cross-stream patterns. The magnitude of these correlations and their persistent shapes across the flows suggest that the spatial separation between regions of concentrated dissipation and production rates is associated with the presence of quasistreamwise vortices in both of these flows. More specifically, they imply that regions of concentrated rates of dissipation are primarily in the cores of the vortices, whereas regions of rates of production are more concentrated on their periphery. © *2007 American Institute of Physics*. [DOI: 10.1063/1.2472510]

I. INTRODUCTION

The significance of regions of highly coherent motion in turbulent flows has been a topic of research for over four decades. The fact that several important flow properties are not randomly distributed in time or space, but instead are spatially and temporally concentrated, has been well documented.[1,2] Arguably the two most widely studied turbulent flows are the zero-pressure-gradient boundary layer and the shear-induced two-stream mixing layer, in part because some approximations of them occur in many engineering applications and in nature, but also due to their simplicity. While their precise origins, geometry, and self-replication are still subjects of considerable research, it is now well established that the predominant structures in the boundary layer are quasistreamwise oriented vortices that sometimes occur in the form of hairpins. The mixing layer is dominated by large spanwise oriented roller vortices and associated smaller quasistreamwise oriented braid vortices.[3] In both types of turbulent flows, these vortical structures appear to strongly influence the spatial and temporal distribution of several important flow properties.

For example, in the two-stream mixing layer, Hussain and Zaman[4] and Loucks[5] have shown, by using averages of hot-wire data conditioned on the passage of these vortices, that the production rate is concentrated at the periphery of the roller vortices where they meet the braid vortices. Additionally and because his multisensor hot-wire probe, described below, provided good estimates of the velocity gradient tensor, Loucks[5] showed that regions of high dissipation rate are concentrated throughout the roller vortices themselves. More recently, Adrian *et al.*[6] used streamwise/wall-normal plane particle image velocimetry (PIV) in a turbulent boundary layer to study the organization of vortices in the logarithmic and outer layers. They found that regions of high Q2 ($u<0$, $v>0$) and Q4 ($u>0$, $v<0$) Reynolds stress occurred in the vicinity of hairpin heads. Ganapathisubramani *et al.*[7] also have investigated vortical structures in a turbulent boundary layer and their relationship to Reynolds stress generation. Using stereoscopic PIV, they found that flow regions identified as legs of hairpin vortices were associated with, but spatially separated from, regions of local Reynolds stress

[a)]Telephone: 301-314-6695. Electronic mail: wallace@eng.umd.edu

(in the sense defined here) with instantaneous values as much as 40 times the local mean value.

In this paper, we consider the spatio-temporal distribution of properties associated with the turbulent kinetic energy (TKE) in both the boundary layer and mixing layer. In particular, we are interested in the correlation between the instantaneous rates of production and dissipation of TKE, and how these correlations might be related to the predominant vortical structures of the flow. It should also now be possible to use PIV data for a study like this one. For example, with data such as those obtained by Ganapathisubramani *et al.*[8] with dual plane PIV utilizing three cameras to estimate the full velocity gradient tensor in streamwise/spanwise planes of a turbulent boundary layer, the temporal correlations reported herein could be replaced with spatial ones.

II. EQUATIONS

The transport equation for TKE is given by

$$\frac{\partial K}{\partial t} + \bar{U}_j \frac{\partial K}{\partial x_j} = -\frac{\partial \bar{U}_i}{\partial x_j} R_{ij} + \epsilon - \frac{1}{\rho}\frac{\overline{\partial p u_i}}{\partial x_j} + \nu \nabla^2 K - \frac{\overline{\partial u_j (u_i^2/2)}}{\partial x_j}, \tag{1}$$

where

$$-\frac{\partial \bar{U}_i}{\partial x_j} R_{ij} = -\frac{\partial \bar{U}_i}{\partial x_j}\overline{u_i u_j} \tag{2}$$

and

$$\epsilon = -\left(\nu\overline{\left(\frac{\partial u_i}{\partial x_j}\right)^2} + \nu\overline{\frac{\partial u_i}{\partial x_j}\frac{\partial u_j}{\partial x_i}}\right) \tag{3}$$

are the production and dissipation rates of TKE (denoted by K), respectively. In Eqs. (1)–(3), U_i and u_i are the instantaneous and turbulent fluctuating velocities in the ith direction. The indices i and j each go through x, y, and z, taken to denote the streamwise, cross-stream, and spanwise directions. The instantaneous streamwise velocity is also interchangeably denoted as U, and the fluctuating velocity components as u, v, and w. Overbars signify time averages, and $\nu = \mu/\rho$ is the kinematic viscosity with μ the molecular viscosity and ρ the density of the fluid. Because Eqs. (2) and (3) define averaged quantities, temporally varying information cannot be obtained from them. However, we can also consider the "instantaneous" production and dissipation rates defined as

$$P = -\frac{\partial \bar{U}_i}{\partial x_j} u_i u_j \tag{4}$$

and

$$D = -\nu\left[\left(\frac{\partial u_i}{\partial x_j}\right)^2 + \frac{\partial u_i}{\partial x_j}\frac{\partial u_j}{\partial x_i}\right]. \tag{5}$$

It is these instantaneous values that we will be treating in this paper, and further discussion of production and dissipation rates will refer to these instantaneous quantities (or the fluctuations about their means). Note that by this definition, the instantaneous production is dominated by the product of a constant, given by the local mean streamwise velocity gradient at a given location, and the local and instantaneous uv product, the average of which is the principal Reynolds shear stress. Note, also, that averaging (4) and (5) yields (2) and (3). Since both the quantities given by Eqs. (4) and (5) are time-varying signals, we can define their temporal cross-correlation coefficient. To calculate this, we first subtract Eqs. (2) and (3) from (4) and (5), respectively, to define quantities p and d, the fluctuating production and dissipation rates. Their correlation coefficient is then given by

$$R_{dp}(\tau) = \frac{\overline{d(t)p(t+\tau)}}{\sqrt{\overline{d^2}}\sqrt{\overline{p^2}}}. \tag{6}$$

Here $R_{dp}(\tau)$ is a temporal cross-correlation of the usual type, giving information about the phase relationship between the two quantities.

For $\tau > 0$, Eq. (6) shifts the production rate forward in time with respect to dissipation rate; for $\tau < 0$, the shift is backward in time. Equivalently, we can invoke Taylor's frozen turbulence hypothesis[10] to define a length $L = \bar{U}\tau$ and say that $\tau > 0$ corresponds to an upstream shift in space of production rate with respect to dissipation rate, while $\tau < 0$ corresponds to a downstream shift. Thus from the temporal location of a correlation maximum, we can infer the approximate spatial relationship between regions of concentrated production and dissipation rate. Furthermore, this spatial relationship can be made nondimensional using a characteristic diffusive length scale $\sqrt{|\tau|\nu}$. The resulting nondimensional length is

$$L' = \frac{\bar{U}\tau}{\sqrt{|\tau|\nu}} = \mathrm{sgn}(\tau)\sqrt{\frac{|\tau|}{\nu}}\bar{U}. \tag{7}$$

III. EXPERIMENTAL ARRANGEMENT

According to the definitions above, the instantaneous production rate can be obtained by measuring the instantaneous streamwise and cross-stream velocity fluctuations, u and v, together with the mean streamwise velocity at each location, from which the velocity gradient can be determined. Simple two-sensor hot-wire probes would suffice for such measurements. However, to measure the instantaneous dissipation rate, all nine velocity gradients in the flow must be determined.

For the boundary-layer data analyzed here, a nine-sensor probe was used by Ong and Wallace.[9] The basic idea for the probe is quite simple. The velocity vector at the center of the array of nine sensors is expanded in a Taylor series to first order, enabling the velocity components cooling each sensor to be expressed in terms of the velocity components at the center of the array of sensors and the six velocity gradients in the cross-stream plane. After calibration, these unknowns are found iteratively for each time step. The three velocity gradients in the streamwise direction are then found using Taylor's hypothesis.

The boundary layer from which these data were taken developed on a flat plate mounted at the horizontal midplane of the 0.5 m × 0.5 m test section of a wind tunnel. The flat

plate has a sharp leading edge; a combination of sand paper and a 5 mm diameter round rod, placed about 2 cm downstream of the leading edge, were used to initialize and stabilize the laminar-turbulent transition of the boundary layer. The measurements were made 3.6 m downstream from the leading edge. For the $U_e=1.8$ m/s speed of the free-stream flow that was maintained for the experiment, the boundary-layer thickness, δ, at the measurement location was about 9.9 cm, and R_θ was approximately 1070. The friction velocity, u_τ, was 0.089 m/s. It was determined using a Clauser fit of the mean velocity data in the logarithmic region and corrected for Reynolds number effects. Measurements were taken at eight different dimensionless heights, $y^+=u_\tau y/\nu$, that began in the buffer layer at $y^+=16$ and ended in the logarithmic layer at $y^+=89$.

The mixing layer data were obtained in an experiment of Loucks[5] with a 12-sensor probe developed earlier by Vukoslavčević and Wallace.[11] The three additional sensors provide some redundancy and additional accuracy, but the principles of operation and data reduction for this probe are similar to those for the nine-sensor probe. The spatial resolution of both of these probes for these experiments was, at worst, about 5–6 Kolmogorov lengths. Other details about the probes and their operation can be found in the references.

To create a mixing layer, a curved splitter plate was mounted in the test section of a wind tunnel with a 4 ft $\times$2 ft cross section and with the free-stream speed set at about 2.5 m/s. The splitter plate divided the flow, accelerating it on one side and decelerating it on the other. The trailing edge of the splitter plate provided a smooth meeting of two turbulent boundary layers and created a mixing layer with a velocity ratio of about 2:1. A screen was placed between the splitter plate and the test section wall on the low-speed side to balance the pressure of the flow in the cross-stream direction, eliminating a vertical velocity and separation at the trailing edge. The measurements were performed 2 m downstream from the trailing edge in the self-similar region of the flow where the momentum thickness θ was about 19.1 mm, and the Reynolds number was about $\mathrm{Re}_\theta=1790$.

IV. RESULTS

A. Boundary layer

A sample time series of the production and dissipation rate signals in the boundary layer at $y^+=26$ is shown in Fig. 1(a). The dissipation rate is nearly always negative because the homogeneous term in Eq. (5), $\nu(\partial u_i/\partial x_j)^2$, dominates. Both signals display some intermittency, but little correlation between them is immediately apparent. The cross-correlation of these two signals for eight positions in the boundary layer, plotted as functions of the time shift τ, are shown in Fig. 2. The curves for positions near the wall have been plotted separately from those further from the wall to highlight the dependence on y^+. The $y^+=35$ correlation curve is included in both plots because it has features common to both. When the same correlations are plotted as functions of the nondimensional length L', their features become better aligned, as shown in Fig. 3. Furthermore, for $35\leqslant y^+\leqslant 73$, the curves

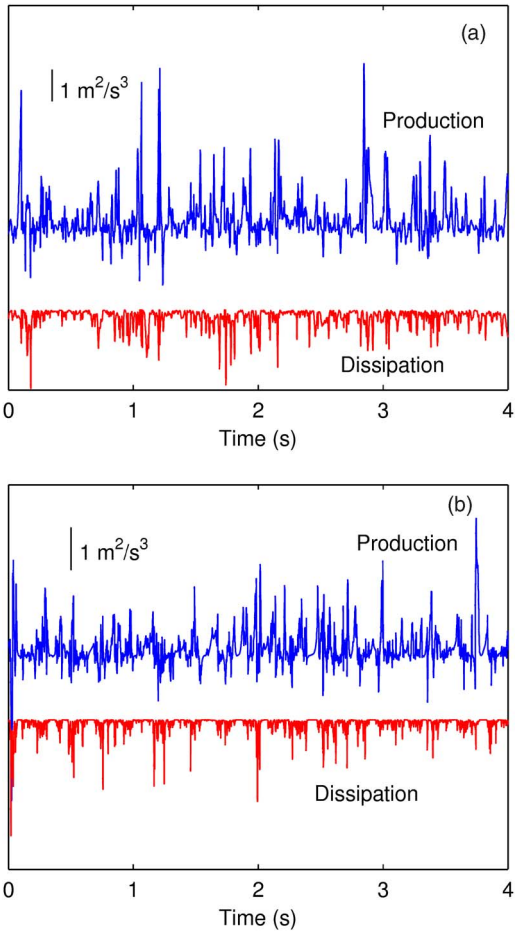

FIG. 1. (Color online) Typical time sequences of instantaneous production and dissipation rates (a) in the boundary layer at $y^+=26$ and (b) in the mixing layer at $y/\theta=2.3$. In each graph, the two signals have been offset from each other for clarity, with production rate above and dissipation rate below.

collapse. We should note that these curves also align when plotted versus the dimensional length, $L=\bar{U}\tau$. This implies that these features are aligned in space, but not in time, without being scaled. Our chosen scaling, L', however, has the advantage of being nondimensional and may be useful when comparing data at different Reynolds numbers.

Several additional interesting features are readily apparent in Fig. 3. First, at each y^+ location, there is a clearly defined correlation peak region that is well above the noise level. This is demonstrated quantitatively by computing the typical variation of the correlation, as measured by its standard deviation, σ. The maximum σ for all probe locations is found to be ± 0.0165, which is indicated by horizontal lines in the upper left of Figs. 3(a) and 3(b). At each probe location, the correlation peaks at more than 8σ, when σ is individually computed for each location. If the production and dissipation rate signals were independent of each other in space and time, no peak in the correlation would likely exceed $\sim\sigma$.

Second, it is clear that the plots are asymmetric with respect to L', and, furthermore, the curves do not always peak at $L'=0$. The fact that the correlation curves peak at small but nonzero L' implies that the regions of production

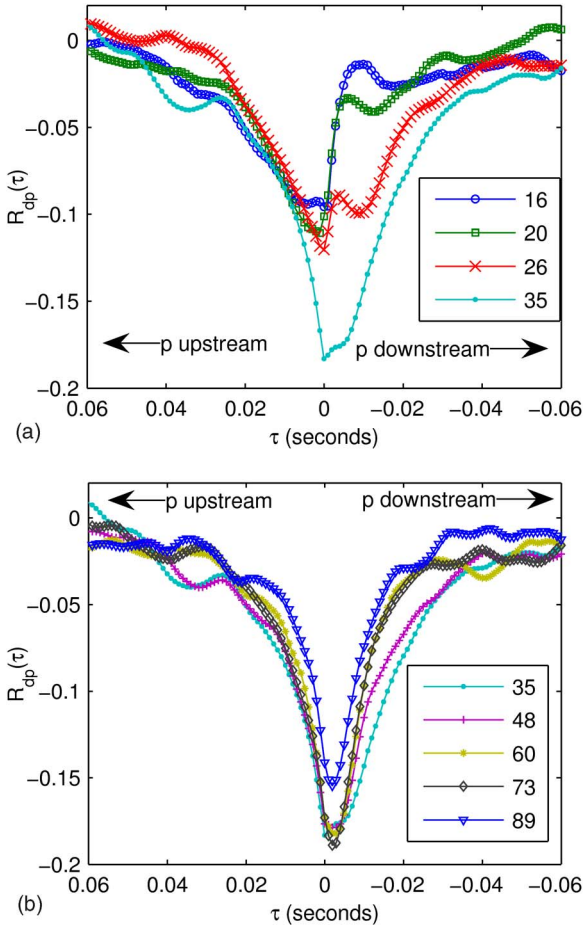

FIG. 2. (Color online) Cross-correlation coefficient of instantaneous production and dissipation rates, as a function of the time shift τ, at different locations in the wall region of the boundary layer: (a) $y^+=16,20,26,35$; (b) $y^+=35,48,60,73,89$. For $\tau>0$, production is upstream of dissipation, and vice versa for $\tau<0$.

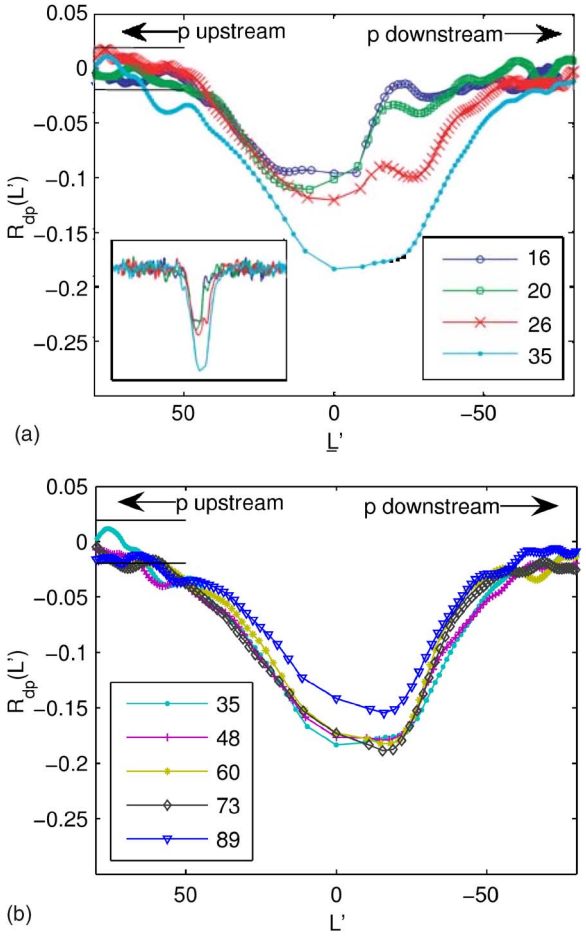

FIG. 3. (Color online) Cross-correlation coefficient of instantaneous production and dissipation rates, as a function of the dimensionless length scale L', at different locations in the wall region of the boundary layer: (a) $y^+=16,20,26,35$; (b) $y^+=35,48,60,73,89$. For $L'>0$, production is upstream of dissipation, and vice versa for $L'<0$. The inset in (a) shows more of the correlation tails in order to illustrate the noise level. The horizontal lines at the upper left in both (a) and (b) show the level of one standard deviation in those long tails, another indication of the noise level.

and dissipation rate typically occur near each other—but not at the same spatial locations. For $y^+<26$, maximum correlation lies at $L'>0$, indicating that regions of concentrated production rate are typically upstream from regions of concentrated dissipation rate. For $y^+>35$, the opposite occurs: maximum correlation lies at $L'<0$, indicating that regions of concentrated production rate are typically downstream from concentrated regions of dissipation rate. Between these regions, in the buffer layer at $y^+=26$ and 35, the correlations curves have peaks around $L'\approx 0$, suggesting a greater coincidence of regions of production and dissipation rate.

Near the wall, an interesting double-peak structure is present, as seen in Fig. 3(a), suggesting that regions of production often appear both upstream and downstream from regions of dissipation. The similarity and alignment between the curves at all y^+ locations indicate the persistence of a pattern over a significant region of the boundary layer.

Using only these time-series data, it is difficult to tell what particular structural features of the turbulence are responsible for creating these distributions. However, some hypotheses can be made from these data. In particular, we can estimate the relative temporal and spatial scales of the motion. The correlation peaks maintain non-negligible magnitude ($>\sigma$) for ~60 ms, as seen in Fig. 2. This τ can be used to compute a more classical "viscous length" scale, defined by $L^+=Lu_\tau/\nu$, where L is a characteristic length and u_τ is the friction velocity. If, as before, we consider $L\approx\bar{U}\tau$ (i.e., the average distance the local flow moves in time $\tau\sim 60$ ms), then L^+ is no greater than about 350. So the turbulent structures that are causing these correlations are small, on the order of a few tens of milliseconds, or no more than a few hundred viscous lengths.

Consider now the interesting double-peak structure discussed above. For example, at $y^+=26$, the spacing between the peaks is roughly 9 ms, corresponding to ~60 viscous lengths, L^+. This distance is roughly the scale of "legs" of hairpin vortices in the wall region.[12,13] These counter-rotating vortices create an alternating pattern of "ejection" and "sweep" type motions, corresponding to Q2 and Q4 Reynolds shear stress and hence high production of TKE at their periphery.[1] If we assume that the dissipation rate is concentrated in the core of these vortices, as Loucks[5] has shown is the case of the large spanwise roller vortices of the

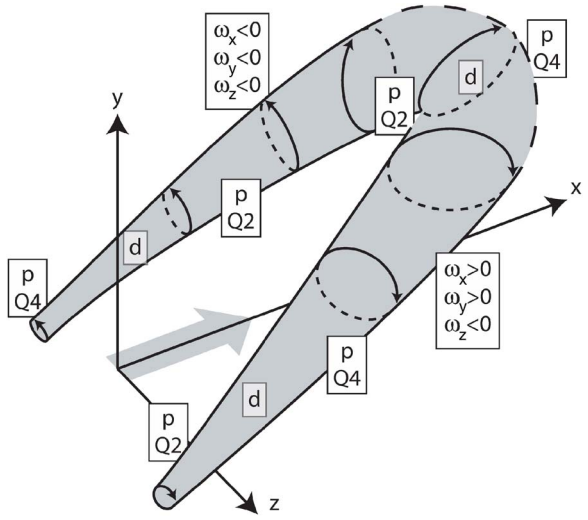

FIG. 4. (Color online) Sketch of the structure of a quasistreamwise vortex. Regions of high production rate are labeled **p**, with the dominant Reynolds shear stress quadrant indicated below each. Regions of high dissipation rate are labeled **d**. Vorticity components, ω_i, have different signs in different regions, as indicated. The mean flow direction is indicated by the large arrow. Dotted lines in the arch of the vortex are meant to imply that not all quasistreamwise vortices are connected to form hairpins.

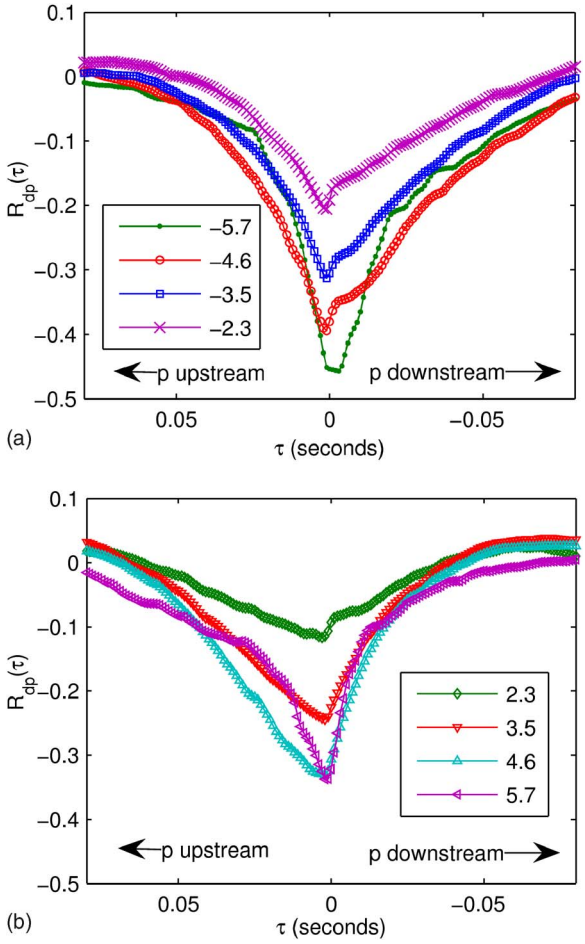

FIG. 5. (Color online) Cross-correlation coefficient of production and dissipation rates, as a function of the time shift τ, at different locations in the mixing layer: (a) $y/\theta=-5.7,-4.6,-3.5,-2.3$; (b) $y/\theta=2.3,3.5,4.6,5.7$. For $\tau>0$, production is upstream of dissipation, and vice versa for $\tau<0$.

two-stream mixing layer, such a configuration could produce two distinct peaks in the correlation coefficient. This would occur if the axes of these vortices are somewhat oblique to the streamwise direction, so that the probe, at a fixed location, senses a pattern of production from ejection (or sweep) motions, then vortex core dissipation, and finally production from sweep (or ejection) motions as these vortices, with either sense of rotation, convect past it. This pattern is illustrated in Fig. 4.

B. Mixing layer

Typical time-series sequences of the production and dissipation rate signals in the mixing layer at $y/\theta=2.3$ are shown in Fig. 1(b). Although these signals appear to be somewhat more correlated than was immediately apparent for the boundary layer, the phase correspondence between them is still not clear. The correlations between production and dissipation rate at eight y/θ positions in the mixing layer are plotted as functions of time τ in Fig. 5. Figure 5(a) presents data from the low-speed side of the layer, and Fig. 5(b) from the high-speed side. As for the boundary layer, when these same correlations are plotted as functions of the nondimensional length L', their features become better aligned, as shown in Fig. 6. Again, just as for the boundary layer, it is transforming the time scale τ to a length scale $\bar{U}\tau$ that better aligns the data. Normalizing it with the diffusive length scale $\sqrt{|\tau|\nu}$ only makes it nondimensional.

Many of the same features that we observed in the boundary-layer plots are also observed in these figures for the mixing layer. The existence of a clear region of correlation significantly higher than the noise level is present, as well as peaks at nonzero L'. As for the boundary layer, the latter implies that production and dissipation do not typically occur at the same spatial locations, but are offset from each other in the streamwise direction. This offset distance is larger, in terms of L', than in the boundary layer. Furthermore, as in the boundary layer, on each side of the mixing layer, the peaks of the curves occur at similar L', implying a persistent pattern in the cross-stream direction. The correlation curves differ significantly from the high-speed to low-speed side. Regions of higher correlation on the low-speed side are much narrower and are shifted somewhat toward $L'<0$, indicating production located downstream of dissipation, although the peak values are near $L'\approx 0$ at several locations. Regions of higher correlation on the high-speed side, by contrast, are very broad and generally located at $L'>0$, indicating production upstream of dissipation. On both sides, the correlation is highest in the range $3.5\leqslant y/\theta\leqslant 5.6$, i.e., toward the outer edges of the mixing layer. The correlation curves near the center plane of the mixing layer do not show these patterns and are not plotted.

Estimating the temporal scale of significant correlation, as was done above for the boundary layer, shows that these features exist on time scales $\approx$80–160 ms. Given the mean flow rate in the mixing layer, such features are too small, temporally, to be associated with the cores of the large roller vortices observed in previous work.[5] The associated braid

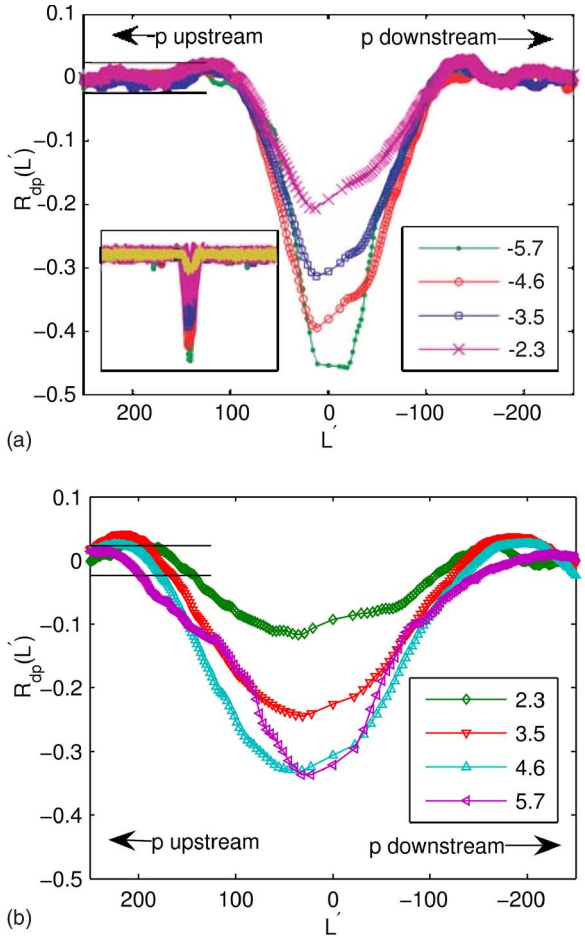

FIG. 6. (Color online) Cross-correlation coefficient of production and dissipation rates, as a function of the dimensionless length scale L', at different locations in the mixing layer: (a) $y/\theta=-5.7,-4.6,-3.5,-2.3$; (b) $y/\theta=2.3,3.5,4.6,5.7$. For $L'>0$, production is upstream of dissipation, and vice versa for $L'<0$. The inset in (a) shows more of the correlation tails in order to illustrate the noise level. The horizontal lines at the upper left in both (a) and (b) show the level of one standard deviation in those long tails, another indication of the noise level.

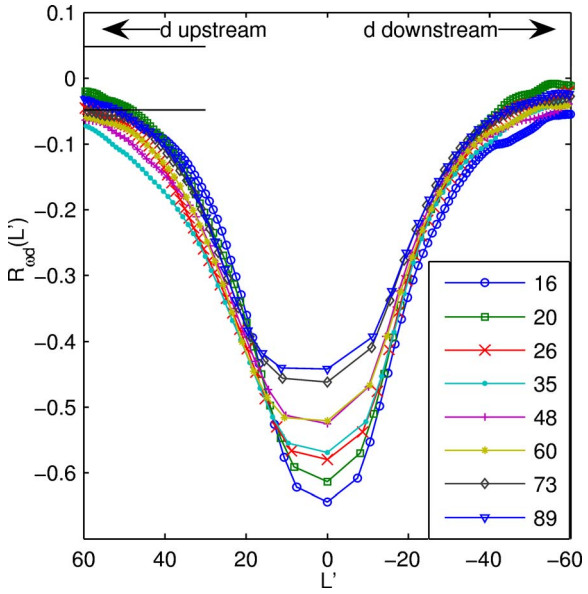

FIG. 7. (Color online) Cross-correlation coefficient of ω_{xy} and dissipation rate, as a function of the dimensionless length scale L', at different y^+ locations in the boundary layer. For $L'>0$, dissipation is upstream of ω_{xy}, and vice versa for $L'<0$. The horizontal line at the upper left shows the level of one standard deviation in the correlation tails.

vortices and the edges of the roller vortices, however, are smaller and might be the flow structures leading to the correlation curve characteristics we find here.

C. Relationship to vortices

The estimates of the temporal and spatial scales presented in the previous sections offer evidence that these unique spatial distributions between production and dissipation rates might be due to relatively small length scale vortical motions. We hypothesized that in the boundary layer, these motions were the result of quasistreamwise oriented "hairpin" vortices, while in the mixing layer, the quasistreamwise oriented "braid" vortices seem to be the most likely candidates. In order to test these hypotheses, initially we calculated the second invariant of the velocity gradient tensor, $Q=-A_{ij}A_{ji}/2$, for incompressible flow, where $A_{ij}=\partial U_i/\partial x_j$ is the velocity gradient tensor. Since Q is made up of the strain rate tensor and the rotation tensor, negative values of Q indicate the dominance of straining motion, while positive values of Q indicate the dominance of vortical motion. This method has been used in the past to identify quasistreamwise oriented vortices in the turbulent mixing layer.[14] Therefore, by computing a time series of Q, and setting all its negative values to zero, we hoped the resulting time series would indicate regions of strong vortical motion. When we correlated this time series with the production and dissipation rate signals, however, the results were inconclusive.

We then decided to use a different identifier of quasistreamwise oriented vortical motions: the projection of the modulus of the vorticity vector on the streamwise (x-y) plane, i.e., $\omega_{xy}=\sqrt{\omega_x^2+\omega_y^2}$. This identifier, which can also be generated as a time series, has the virtue of being insensitive to the angle of inclination of the vortices to the wall. Correlating it with the fluctuating dissipation rate, $d(t)$, and with the fluctuating production rate, $p(t)$, results in the correlation coefficients,

$$R_{\omega d}(\tau)=\frac{\overline{\omega_{xy}(t)d(t+\tau)}}{\sqrt{\overline{\omega_{xy}^2}}\sqrt{\overline{d^2}}}, \tag{8}$$

$$R_{\omega p}(\tau)=\frac{\overline{\omega_{xy}(t)p(t+\tau)}}{\sqrt{\overline{\omega_{xy}^2}}\sqrt{\overline{p^2}}}, \tag{9}$$

which can also be plotted as functions of L'.

Plots of the $R_{\omega d}$ correlations for all the measurement locations in the boundary layer are shown in Fig. 7. The correlation levels are quite high with the significant levels of correlation occurring over length scales of $L'\approx\pm 60$ for $|R_{\omega d}|>\sigma$. Furthermore, the peaks of the correlation functions for all locations are centered on $L'\approx 0$, indicating that the vortical motions and concentrations of dissipation rate are nearly coincident. This coincidence and the high correlation levels are perhaps not so remarkable when it is recalled that

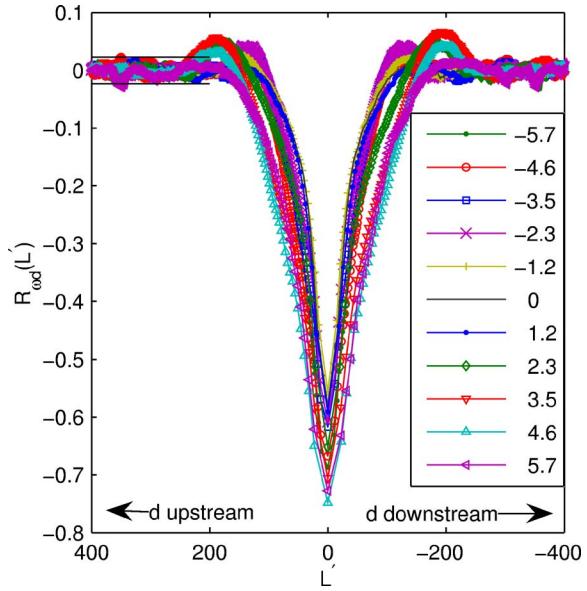

FIG. 8. (Color online) Cross-correlation coefficient of ω_{xy} and dissipation rate, as a function of the dimensionless length scale L', at different y/θ locations in the mixing layer. For $L'>0$, dissipation is upstream of ω_{xy}, and vice versa for $L'<0$. The horizontal lines at the upper left show the level of one standard deviation in the correlation tails.

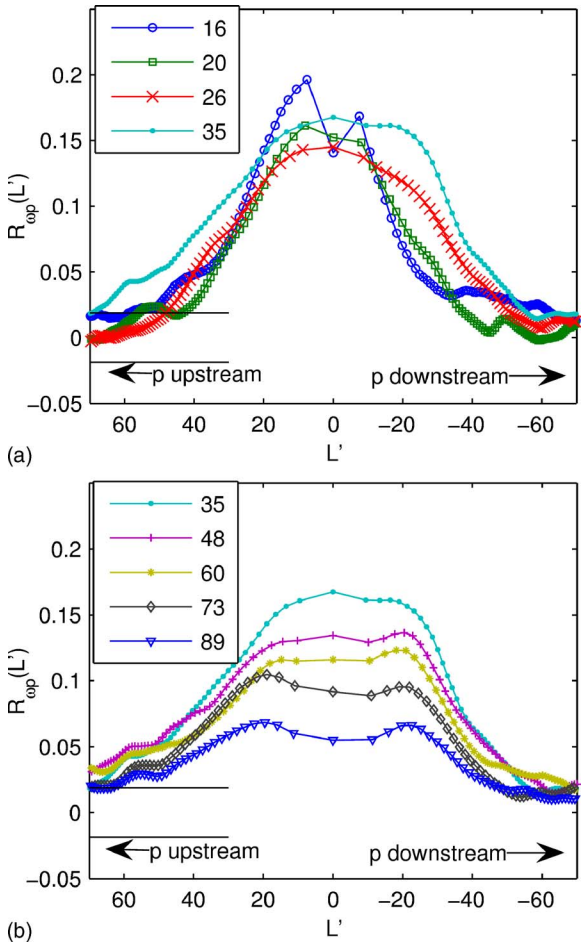

FIG. 9. (Color online) Cross-correlation coefficient of ω_{xy} and production rate, as a function of the dimensionless length scale L', at different locations in the boundary layer: (a) $y^+=16,20,26,35$; (b) $y^+=35,48,60,73,89$. For $L'>0$, production is upstream of ω_{xy}, and vice versa for $L'<0$. The horizontal lines at the lower left in both (a) and (b) show the level of one standard deviation in the correlation tails.

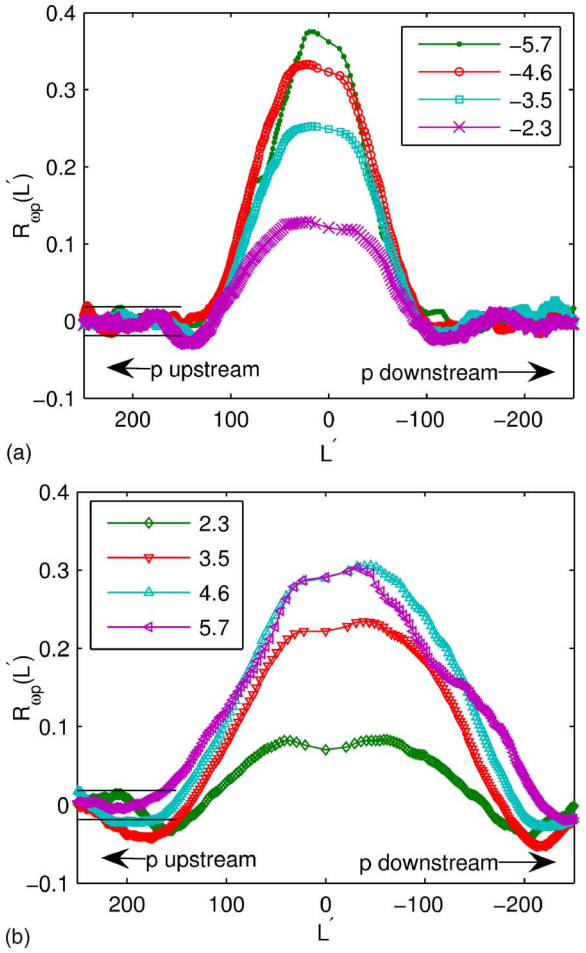

FIG. 10. (Color online) Cross-correlation coefficient of ω_{xy} and production rate, as a function of the dimensionless scale L', at different locations in the mixing layer: (a) $y/\theta=-5.7,-4.6,-3.5,-2.3$; (b) $y/\theta=2.3,3.5,4.6,5.7$. For $L'>0$, production is upstream of ω_{xy}, and vice versa for $L'<0$. The horizontal lines at the lower left in both (a) and (b) show the level of one standard deviation in the correlation tails.

enstrophy is closely related to dissipation rate, being exactly equal to it in homogenous turbulence. Some similar conclusions can be drawn for the mixing layer from the $R_{\omega d}$ correlation coefficient versus L' plots for all measurement locations, as shown in Fig. 8. The correlation levels are similarly high and the peaks are centered on zero spatial separation. The length scales of significant correlation levels in the mixing layer are about twice those in the boundary layer.

When the fluctuation production rate, p, is correlated with ω_{xy}, the correlation levels are not so high, but they are still quite significant, as seen in Fig. 9 for the boundary layer. Notably, $R_{\omega p}$ has a pronounced double peak at $y^+=16$ in the buffer layer and less pronounced but still quite observable double peaks in the logarithmic layer. Additionally, the spatial separation of these peaks increases with distance from the wall. These observations are consistent with the hypothesis that greater concentration of production rate occurs on either side at the periphery of quasistreamwise vortices that are skewed somewhat to the x-y plane, as described above and illustrated in Fig. 4. The fact that the length scale of the double-peak structure increases with distance from the wall

is also consistent with the generally held view that the size of these vortices increases with distance from the wall.

On the high-speed side of the mixing layer, the $R_{\omega p}$ correlations show similar features to those for the boundary layer, as seen in Fig. 10(b). The double-peak structure is discernible, although not so pronounced, but its length scale is larger than in the boundary layer. The peak correlation values occur downstream on the high-speed side, but are shifted upstream on the low-speed side where the double-peak structure does not occur [Fig. 10(a)]. Finally, the correlation levels of $R_{\omega p}$ are very low for positions near the mixing layer centerline (not shown) in contrast to the high levels of $R_{\omega d}$ throughout the mixing layer. This suggests that the regions of concentration of production rate are not only upstream and downstream of the vortex cores, but are also offset away from the mixing layer centerline as was observed by Hussain and Zaman[4] and Loucks.[5]

V. CONCLUSION

We have presented a novel data analysis technique for studying the spatial distribution of instantaneous production and dissipation rates in turbulent shear flows and their relationship to vortical structures. Cross-correlating fluctuating signals that measure the strength of the production and dissipation rates revealed unique spatial distributions in both a turbulent boundary layer and a turbulent mixing layer. Correlating these fluctuating signals with a fluctuating vortex identifier revealed recurring spatial features. These features are consistent with the presence in both flows of quasistreamwise vortices skewed somewhat to the streamwise plane. These vortices induce Reynolds shear stress motions (and thus turbulent kinetic energy production) at their peripheries, while dissipating the energy in their interiors. Well-resolved DNS and PIV data providing the full spatial distributions and instantaneous realizations of production and dissipation rate in boundary and mixing layers would, undoubtedly, reveal much more about their kinematical and dynamical relationships to the organized vortical structures that are so important to understanding these generic turbulent flows.

[1] S. K. Robinson, "Coherent motions in the turbulent boundary layer," Annu. Rev. Fluid Mech. **23**, 601 (1991).
[2] P. S. Bernard and J. M. Wallace, *Turbulent Flow: Analysis, Measurement, and Prediction* (John Wiley & Sons, Hoboken, NJ, 2002).
[3] L. P. Bernal and A. Roshko, "Streamwise vortex structure in plane mixing layers," J. Fluid Mech. **170**, 499 (1986).
[4] A. K. M. F. Hussain and K. B. M. Q. Zaman, "An experimental study of organized motions in the turbulent plane mixing layer," J. Fluid Mech. **159**, 85 (1985).
[5] R. B. Loucks, "An experimental examination of the velocity and vorticity fields in a plane mixing layer," Ph.D. dissertation, University of Maryland (1998).
[6] R. J. Adrian, C. D. Meinhart, and C. D. Tomkins, "Vortex organization in the outer region of the turbulent boundary layer," J. Fluid Mech. **422**, 1 (2000).
[7] B. Ganapathisubramani, E. K. Longmire, and I. Marusic, "Characteristics of vortex packets in turbulent boundary layers," J. Fluid Mech. **478**, 35 (2003).
[8] B. Ganapathisubramani, E. K. Longmire, and I. Marusic, "Dual-plane PIV technique to determine the complete velocity gradient tensor in a turbulent boundary layer," Exp. Fluids **39**, 222 (2003).
[9] L. Ong and J. M. Wallace, "Joint probability density analysis of the structure and dynamics of the vorticity field of a turbulent boundary layer," J. Fluid Mech. **367**, 291 (1998).
[10] G. I. Taylor, "Production and dissipation of vorticity in a turbulent fluid," Proc. R. Soc. London, Ser. A **164**, 15 (1938).
[11] P. Vukoslavčević and J. M. Wallace, "A 12-sensor hot-wire probe to measure the velocity and vorticity vectors in turbulent flow," Meas. Sci. Technol. **7**, 1451 (1996).
[12] C. R. Smith and S. P. Metzler, "The characteristics of low-speed streaks in the near-wall region of a turbulent boundary layer," J. Fluid Mech. **129**, 27 (1983).
[13] C. R. Smith and S. P. Schwartz, "Observation of streamwise rotation in the near-wall region of a turbulent boundary layer," Phys. Fluids **26**, 641 (1983).
[14] E. Balaras, U. Piomelli, and J. M. Wallace, "Self-similar states in turbulent mixing layers," J. Fluid Mech. **446**, 1 (2000).